Inorganic Chemistry

Article

pubs.acs.org/IC

Absorption and Electrochemical Properties of Cobalt and Iron Phthalocyanines and Their Quaternized Derivatives: Aggregation Equilibrium and Oxygen Reduction Electrocatalysis

Thiago Teixeira Tasso, Taniyuki Furuyama, and Nagao Kobayashi*

Department of Chemistry, Graduate School of Science, Tohoku University, Sendai 980-8578, Japan

Supporting Information

ABSTRACT: The synthesis and investigation of the electronic properties of Co(II) and Fe(II)tetrakis(pyridine-3-yloxy)phthalocyanines, as well as the respective quaternized complexes, are reported here. After quaternization reaction, the compounds showed increased solubility in water, and their aggregation equilibrium was analyzed by varying the solution concentration, pH, and composition. Cyclic voltammograms of the four compounds showed both metal and ring centered redox processes, with the former being highly sensitive to methylation of the pyridyl groups. The catalytic effect of the phthalocyanines adsorbed on glassy carbon electrodes in the oxygen reduction reaction (ORR) was investigated by cyclic voltammetry (CV) and rotating disk voltammetry (RDV). The highest catalytic activities were observed for the Fe(II) complexes in alkaline media, and a 2 + 2 mechanism, which consists of a first complete O_2 to H_2O_2 process and a subsequent incomplete H_2O_2 to H_2O process, is proposed.

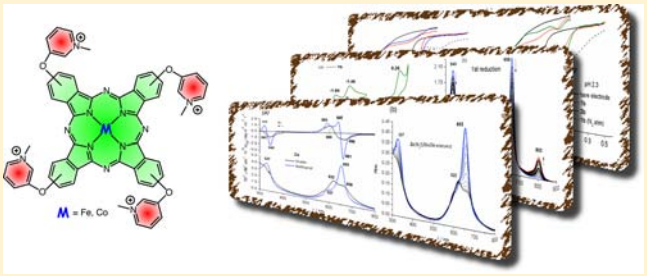

INTRODUCTION

Since their discovery in 1907, phthalocyanines (Pcs) and derivatives have been intensively studied for application in a variety of areas. In addition to the chemical and thermal stability and semiconductivity, conferred by the highly conjugated π electron system, the macrocyclic properties can be tuned by insertion of different elements and peripheral groups onto the ring.[1] Such versatility allows their recent usage to range from electrochromic devices,[2] such as displays, to medical purposes, such as photodynamic therapy (PDT).[3]

Phthalocyanines containing redox-active metals such as iron and cobalt are also known to catalyze many important reactions. One reaction, which has received increased attention recently, is the oxygen reduction reaction (ORR), which consists of the reduction of molecular oxygen to water. This can be achieved in a single four-electron reduction step or in two steps of two electrons each, yielding H_2O_2 as an intermediate. Since O_2 is abundant in air and water is the final product, the ORR has been applied for clean energy production, such as in air-lithium batteries and fuel cells.[4] The efficiency of these systems is highly dependent on the catalytic effectiveness of the cathode toward ORR, and recently, cobalt and iron complexes have been investigated as potential substitutes for expensive materials such as platinum and gold.[5]

CoPc was reported as the first alternative cathode to noble metals,[6] and its activity on electrode surfaces and at liquid−liquid interfaces has been recently studied.[7] FePc has also been investigated, showing good results as a material for both oxygen and hydrogen peroxide operated fuel cells.[8] Other tetrapyrrolic complexes, such as porphyrins and corroles, have also shown catalytic activity toward ORR. The pyrolized tetraphenylporphyrin of iron(II) (FeTPP) deposited on carbon black, for example, was reported to achieve approximately half the performance of platinum for the same amount of metal.[9] Most recently, cobalt(III) corroles were reported to catalyze the ORR at very anodic potentials, with increased maximum power density of the cell.[10]

In addition to fuel cell operation, ORR is also important for microorganism growth control and the oxidation of molecules such as thiols, which are desired for antibacterial[11] and deodorant purposes. In these cases, the introduction of substituent groups which can increase the Pc's solubility in polar solvents and also bind to fibers and other substrates is often required. Shirai and co-workers demonstrated the catalytic activity of di-, tetra-, and octacarboxyphthalocyanines containing different metal centers for the oxidation of 2-mercaptoethanol in aqueous solution. They found that the octa-substituted complexes of Co(II) and Fe(III) had the most remarkable catalytic effect.[12] Although there are a considerable number of reports on Pcs containing negatively charged groups, only a few articles have so far reported the properties of the cationic species. In addition, positively charged Pcs show better cell uptake from both gram positive and gram negative bacteria,[11] and hence enhanced inactivation efficiency.

As mentioned above, since the discovery of CoPc as a potential catalyst in energy production systems, increased attention has been given to tetrapyrrolic complexes containing

Received: January 27, 2013
Published: August 5, 2013

   dx.doi.org/10.1021/ic4002048 | *Inorg. Chem.* 2013, 52, 9206−9215

cobalt and iron ions, due to their increased catalytic activity in ORR. However, much has yet to be explored in relation to these kinds of systems since the versatility of these macrocycles allows their properties to be tuned and enhanced through different ways. Thus, in this Article, we report the synthesis and electronic properties of the Co(II) and Fe(II) tetrasubstituted phthalocyanines **1a** and **1b**, and their quaternized cationic derivatives, **2a** and **2b** (Figure 1), as well as their efficiency for

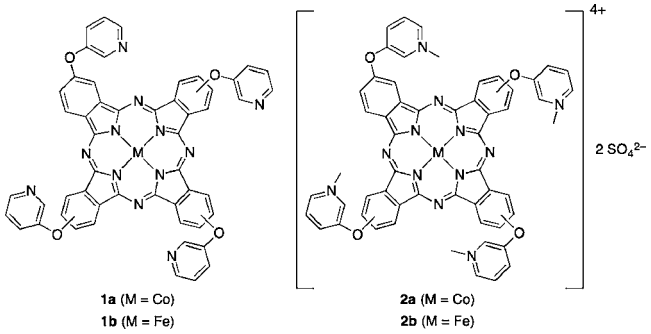

Figure 1. Schematic representation of the structure of the phthalocyanines studied in this work.

heterogeneous catalysis in ORR. Ionic Pcs are known to easily form aggregates in polar solvents, which are usually undesirable for various applications, and hence the aggregation equilibrium of **2a** and **2b** was also investigated. Similar water-soluble metalloPcs (metal = Zn, Si, etc.) containing quaternized pyridyl groups have already been reported in the literature as potential photosensitizers for medical treatment;[13] however, the corresponding cobalt and iron complexes and their use as catalysts for the ORR are reported here for the first time.

EXPERIMENTAL SECTION

Materials and Instrumentation. Unless otherwise noted, solvents and reagents were purchased from Tokyo Kasei Co. and Wako Chemicals Co. and were used after appropriate purification (distillation or recrystallization). Pyridine and DMF used for spectroscopic and voltammetric measurements were previously dried by refluxing with CaH_2 for several hours, followed by distillation.

Electronic absorption spectra were recorded on a JASCO V-570 spectrophotometer. Magnetic circular dichroism (MCD) spectra were obtained on a JASCO J-725 spectrodichrometer equipped with a JASCO electromagnet capable of producing magnetic fields of up to 1.03 T (1 T = 1 Tesla) with both parallel and antiparallel fields. The magnitudes were expressed in terms of molar ellipticity per tesla ($[\theta]_M$/deg dm^3 mol^{-1} cm^{-1} T^{-1}). FT-IR spectra were recorded on a JASCO (FT/IR-4100) by dispersing the samples in KBr pellets. ^{1}H NMR spectra were obtained on a Bruker AVANCE 500 spectrometer, and unless otherwise noted, spectra were recorded in $CDCl_3$. Chemical shifts are expressed in δ (ppm) values. The spectra were referenced to the residual solvent as an internal standard. MALDI-TOF and ESI mass spectra were recorded on AB Sciex (4800 Plus) and JEOL (JMS-T100LP) models, respectively. High-resolution mass spectra (HRMS) were recorded on a Bruker Daltonics Apex-III spectrometer. Cyclic voltammetry (CV) and differential pulse voltammogram (DPV) measurements were recorded with a Hokuto Denko HZ5000 potentiostat under a nitrogen atmosphere in solutions with 0.1 M of tetrabutylammonium perchlorate (TBAP) as supporting electrolyte. Measurements were made with a glassy carbon (GC) electrode (area = 0.07 cm^2), an Ag/AgCl reference electrode, and a Pt wire counter electrode. The concentration of the solution was fixed at 1.0 mM, and the sweep rates were set to 100 mV/s. The ferrocenium/ferrocene couple (Fc^+/Fc) was used as an internal standard. For ORR experiments, buffer solutions were prepared following the procedure described by Britton and Robinson.[14] The solutions were saturated with oxygen by bubbling air for several minutes before measurement. The GC electrode was coated with the samples by immersing it in the sample solution (0.25 mg/L) for five minutes, rinsing with the same solvent, and drying in air. Rotating disk electrode (RDE) experiments were performed in a similar system as described above; however, a rotating glassy carbon electrode of 0.196 cm^2 area and a Hokuto Denko HR-300 were used for varying the rotation rates. Spectroelectrochemical measurements were performed in a quartz cell of 1 mm optical length with a Pt grid as working electrode, Pt as counter electrode, and an Ag/AgCl reference electrode, all connected to a Hokuto Denko HA-501 potentiostat. TBAP solution (0.3 M) was used as supporting electrolyte.

Synthesis of 3-(Pyridine-3-yloxy)benzenephthalonitrile.[15] 4-Nitrophthalonitrile (4.0 mmol, 0.69 g) and 3-hydroxypyridine (6.0 mmol, 0.50 g) were stirred with 40 mL of dry DMSO at 90 °C, while 1.0 g of K_2CO_3 was added every 5 min until 8 additions had been completed. The mixture was heated for a further 45 min and allowed to cool to room temperature. After adding 100 mL of water, the mixture was extracted with $CHCl_3$ and the organic layer washed with Na_2CO_3 (5%) and dried over $MgSO_4$. After solvent removal, the residue was recrystallized from methanol. Yield: 0.65 g (74%).

^{1}H NMR ($CDCl_3$) δ (ppm): 8.81−8.63 (m, 1H, Py), 8.50 (t, 1H, Py), 7.78 (d, 1H, Py), 7.45−7.47 (m, 2H, Ar), 7.34 (d, 1H, Py), 7.30 (d, 1H, Ar). ESI-TOF-MS m/z Calcd for ([2 M + Na]$^+$): 465.1. Found: 465.1.

*Synthesis of Co(II)tetrakis(pyridine-3-yloxy)phthalocyanine (**1a**).*[16] The above nitrile (0.90 mmol, 0.20 g) and $Co(OAc)_2$ (0.25 mmol, 43 mg) were heated in 15 mL of ethylene glycol at 200 °C for 5 h. The reaction mixture was then allowed to cool, poured over 30 mL water, and filtered. The dark blue solid was washed with water, acetone, dichloromethane, and cold methanol. Further purification was achieved by washing the solid with chloroform, ethyl acetate, THF, and diethyl ether in a Soxhlet extractor for several hours. Yield: 0.16 g (74%).

FTIR (KBr, cm^{-1}): 3059 (ν C−H), 1612 (ν C−C), 1520, 1471 (ν C−N), 1235 (ν C−O), 1095, 1058 (ν C−O−C), 754, 705 (δ C−H). HR-MALDI-TOF-MS m/z Calcd for $C_{52}H_{28}N_{12}O_4Co$ (M^+): 943.16830. Found: 943.16832. UV−vis (pyridine) λ_{max} ($\varepsilon \times 10^{-4}$): 340 nm (5.3), 599 nm (1.9), 660 nm (6.4).

*Synthesis of Fe(II)tetrakis(pyridine-3-yloxy)phthalocyanine (**1b**).* Synthesis and purification of **1b** were performed by the same procedure described for **1a**, using in this case $FeSO_4$ (0.025 mmol, 0.038 g) as the metal salt, and the reaction was carried out under a nitrogen atmosphere. Yield: 0.067 g (32%).

FTIR (KBr, cm^{-1}): 3132 (ν C−H), 1611 (ν C−C), 1510, 1471 (ν C−N), 1242 (ν C−O), 1100, 1057 (ν C−O−C), 754, 668 (δ C−H). ^{1}H NMR (pyridine-d_5) δ (ppm): 9.56−9.52 (m, 2H, Pc), 9.42−9.38 (m, 2H, Pc), 9.26−9.16 (dd, 4H, Pc), 9.00−8.91 (dd, 4H, pyridyl), 8.64−8.57 (m, 4H, pyridyl), 7.82−7.75 (m, 4H, Pc), 7.66−7.54 (m, 4H, pyridyl), 7.36−7.28 (m, 4H, pyridyl). HR-MALDI-TOF-MS m/z Calcd for $C_{52}H_{28}N_{12}O_4Fe$ (M^+): 940.17005. Found: 940.17009. UV−vis (pyridine) λ_{max} ($\varepsilon \times 10^{-4}$): 340 nm ($\varepsilon$ = 10.0), 418 nm (2.4), 597 nm (3.3), 664 nm (12.0).

*Synthesis of Quaternized **1a** (**2a**).*[17] Methylation of the pyridyl groups was achieved by heating **1a** (0.16 mmol, 0.15 g) in 0.5 mL of dried DMF to 120 °C, and adding a few drops of dimethyl sulfate to the mixture. The reaction was allowed to proceed for 12 h at 120 °C. After cooling to room temperature, the mixture was poured into hot acetone and the resultant solid collected by filtration and washed with more acetone. Further purification was achieved by successive washing with chloroform, dichloromethane, ethyl acetate, and methanol in a Sohxlet extractor. Yield: 0.16 g (84%).

FTIR (KBr, cm^{-1}): 3132 (ν C−H), 1611 (ν C−C), 1502, 1408 (ν C−N), 1276, 1098 (ν S−O), 1059 (ν C−O−C) 753, 674 (δ C−H). HR-ESI-TOF-MS m/z Calcd for $C_{56}H_{40}N_{12}O_4Co$ (M^{4+}): 250.81514. Found: 250.81513.

*Synthesis of Quaternized **1b** (**2b**).* Compound **1b** (0.06 mmol, 0.059 g) and a few drops of dimethyl sulfate were reacted as described

dx.doi.org/10.1021/ic4002048 | Inorg. Chem. 2013, 52, 9206−9215

in the procedure for **2a**, following the same purification steps. Yield: 0.035 g (47%).

FTIR (KBr, cm^{-1}): 3056 (ν C−H), 1612 (ν C−C), 1503, 1405 (ν C−N), 1277, 1127 (ν S−O), 1060 (ν C−O−C) 751, 672 (δ C−H). ^{1}H NMR (D_2O) δ (ppm): 7.45−9.20 (m, 28H), 4.32−4.52 (m, 12H). ESI-TOF-MS m/z Calcd for $C_{56}H_{40}N_{12}O_4Fe$ (M^{4+}): 255.1. Found: 254.7.

RESULTS AND DISCUSSION

Preparation of Phthalocyanines. Phthalocyanines **1a** and **1b** could be obtained in good yields by the simple one-step reaction of tetramerization of the nitrile in ethylene glycol. ^{1}H NMR signals of **1b** appeared in the same region as those observed for diamagnetic metalated Pcs, providing strong evidence that the oxidation state of Fe is +2. The spectrum also showed that these macrocycles were obtained as a mixture of isomers, but isomer separation was not attempted in this work. Both **1a** and **1b** showed excellent solubility in pyridine, poor solubility in DMF or DMSO, and insolubility in many other organic solvents. Quaternization of the pyridyl rings was achieved by heating these macrocycles in a strong methylating agent such as dimethyl sulfate, and partially methylated coproducts were not detected in the ESI mass spectra. After the quaternization reaction, water-solubility was achieved for both the cobalt and iron complexes. The sulfate salts of **2a** and **2b** were poorly soluble in DMF. Counteranion exchange with sodium perchlorate was carried out, producing DMF-soluble quaternized Pcs as the perchlorate salts before electrochemical data were collected.

UV−Visible and MCD Spectra. Figure 2 shows the absorption and MCD spectra of **1a** and **1b** in pyridine. Both complexes show a single intense absorption in the 600−700 nm region (Q-band) which is typical of metalloPcs with D_{4h} symmetry. Since this transition is also sensitive to aggregation, the absence of additional strong bands in this region indicates that these complexes are monomeric in pyridine solution.[18] The strong absorption in the UV region (Soret or B band) is also characteristic of these macrocycles, and similar to the Q-band, the value of its extinction coefficient value is highly dependent on the metal coordinated to the ring. This property can be seen in the ε values of both the Soret and Q bands of **1b**, which are approximately twice those of **1a**. The absorption spectrum of the iron complex also shows an extra band at 419 nm, which can be assigned to an Fe → Pc(π*) MLCT process.[1a] To verify the coordination number of the central iron, an excess of *N*,*N*-dimethyl-4-aminopyridine (DMAP) was added to a pyridine solution of **1b**. DMAP has a stronger σ donating property than pyridine, and pentacoordinated species can be transformed into hexacoordinated species by its addition. However, the resulting spectrum was the same as the pure **1b** solution, and **1b** in pyridine is concluded to exist mostly as the hexacoordinated complex $FePc(py)_2$. The MCD spectra of both **1a** and **1b** revealed Faraday *A*-terms for both the Soret and Q bands, thus providing experimental supporting evidence that the excited state is orbitally degenerate.[1] This is evidence of the high chromophore symmetry of the metalloPc ring.

Aggregation Properties under Various Conditions. Aggregation of Pcs in aqueous solution is usually an undesirable process due to a resulting decrease in some of the functions required for many applications. Therefore, the aggregation properties of quaternized Pcs were studied in a series of water/organic solvent mixtures.[19] Figure 3a shows the absorption and

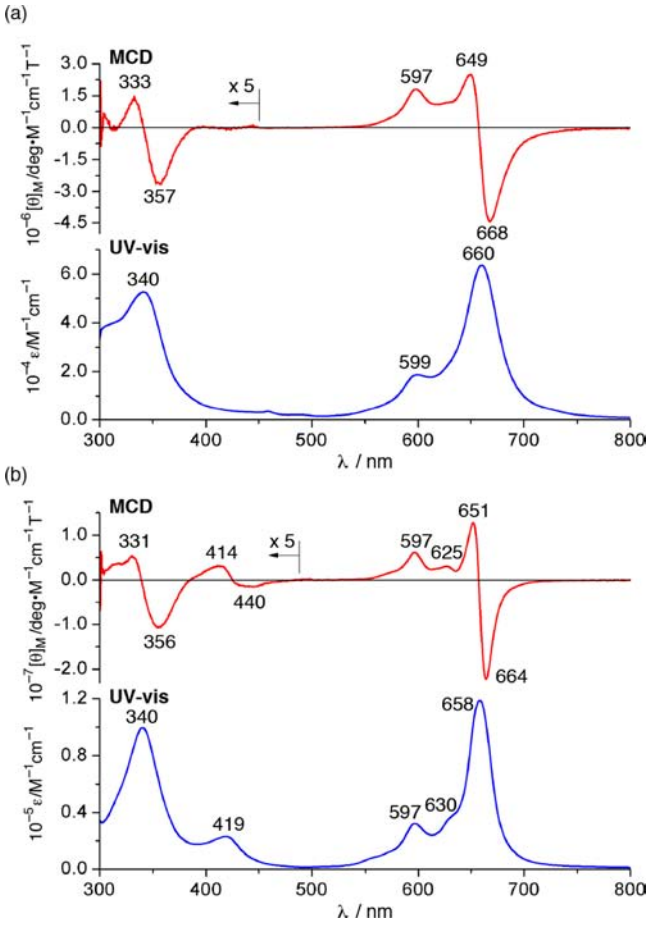

Figure 2. Absorption and MCD spectra of compounds **1a** (a) and **1b** (b) in pyridine.

MCD spectra of **2a** in water and methanol solutions (ca. 8 × 10^{-6} mol/L). The absorption spectrum in methanol shows clear, single Soret and Q band peaks at 327 and 653 nm, respectively, while the MCD spectrum shows dispersion-type Faraday *A*-terms corresponding to both peaks, which is characteristic of monomeric metalloPc species. On the other hand, the absorption spectrum in water is very different from the spectrum in methanol, with two broad peaks appearing at 659 and 622 nm in the Q-band region. The appearance of a blue-shifted absorption (622 nm) in the electronic spectrum, relative to the monomer peak (653 nm), suggests that the macrocycles are arranged in a face-to-face position (H-type) in the aggregate, whereas red-shifts are expected for head-to-head or head-to-tail arrangements (J-type).[20] With increasing content of methanol in the mixtures, there is a sharp increase in the monomer band absorbance (653 nm), followed by a decrease in the blue-shifted band (622 nm), indicating dissociation of the dimer (Figure 3b,c). Sharp isosbestic points in the spectra point to the existence of a single equilibrium in solution, and thus, formation of higher aggregates can be ruled out. The intersection point between the curves of the inset plot shows that, in the mixture containing water/methanol in a 43/57 (v/v) ratio, 50% of the phthalocyanine molecules are dimerized. In the MCD spectrum in water, dimer and monomer coexist in solution, and a Faraday *A*-term can be observed corresponding to the absorption peak at 622 nm, strongly suggesting that the symmetry of the dimer is either/or both D_{4h} and D_{4d}.[21] Therefore, **2a** appears to form mostly H-

dx.doi.org/10.1021/ic4002048 | Inorg. Chem. 2013, 52, 9206−9215

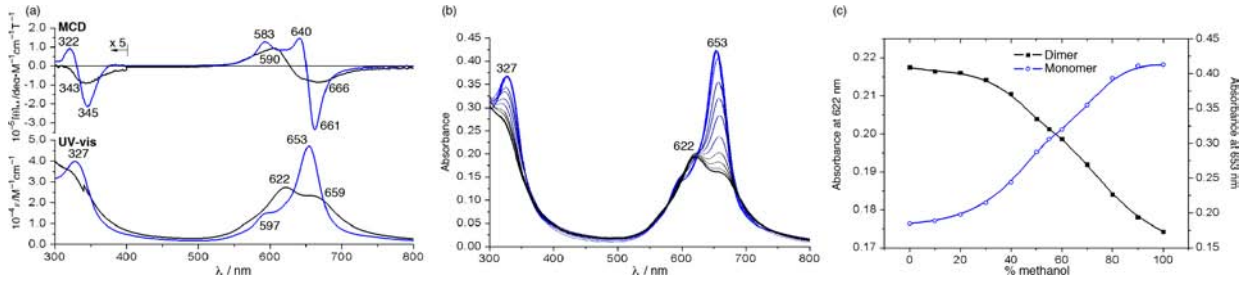

Figure 3. (a) Absorption and MCD spectra of **2a** in pure water (black line) and pure methanol (blue line) solutions. (b) Absorption spectra of **2a** in solutions with different proportions of water/methanol and (c) plot of the absorbance values of the monomer and dimer bands of **2a** in different water/methanol mixtures.

type aggregates in solution, since a J-type aggregation should result in a red-shift in the absorption spectrum, while a Faraday *A*-term would not be expected in the MCD spectrum.

Further studies on the aggregation equilibrium of **2a** were performed using organic solvents other than methanol (acetonitrile, THF, and dioxane), within a range of polarity values. The organic solvent percentages taken from the intersection points of each graph were plotted against the solvent polarity parameter (E_T^N) [Figure S1 in the Supporting Information (SI)].[22] This plot clearly shows that the proportion of organic solvent needed to disaggregate the species in solution increases with increasing solvent polarity. This correlation is reasonable, considering that the highly hydrophobic phthalocyanine rings tend to approach each other in polar media.

The central element coordinated to the ring has also considerable influence over the Pc dimer−monomer equilibrium. Although compound **2b** in water also shows dimer and monomer absorptions in the spectrum at 633 and 688 nm, respectively, the proportion of each species is barely affected by mixing organic solvents into the solution (Figure S2). Thus, a different strategy was adopted to disaggregate this compound in solution. The use of cyclodextrins (CDs) for disaggregation of porphyrins and phthalocyanines in water has been previously reported.[23] In a similar manner, addition of *β*-CD to the aqueous solution of **2b** disturbed the monomer−dimer equilibrium, as can be seen by the increase of the monomer band and decrease of the dimer band absorbance (Figure 4a). However, complete disaggregation was not achieved, even with the addition of a large excess. Better results were obtained when the polymer of *β*-CD (poly *β*-CD) was used instead of the monomeric *β*-CD, as shown by the absorption spectrum in the same plot. When different amounts of poly *β*-CD were added to solutions containing the same concentration of **2b**, maximum disaggregation was obtained with a polymer concentration of 50 mg/mL (Figure 4b).

The influence of the concentration of **2a** and **2b**, as well as the pH of the solution, on the aggregation equilibrium of these compounds was also investigated. As expected, the proportion of dimer of both macrocycles increases with increasing concentration, reaching a constant value at approximately 3×10^{-5} M (Figure S3). However, the equilibrium of **2b** is less sensitive to concentration variations, since the initial increase of its dimer proportion is much less notable than for **2a**. Differences in the aggregation behavior of these phthalocyanines were also found when they were dissolved in buffer solutions containing a range of pH values. No significant changes were observed in the absorption spectra of **2a** in acidic media, and the compound showed stability even at low pH

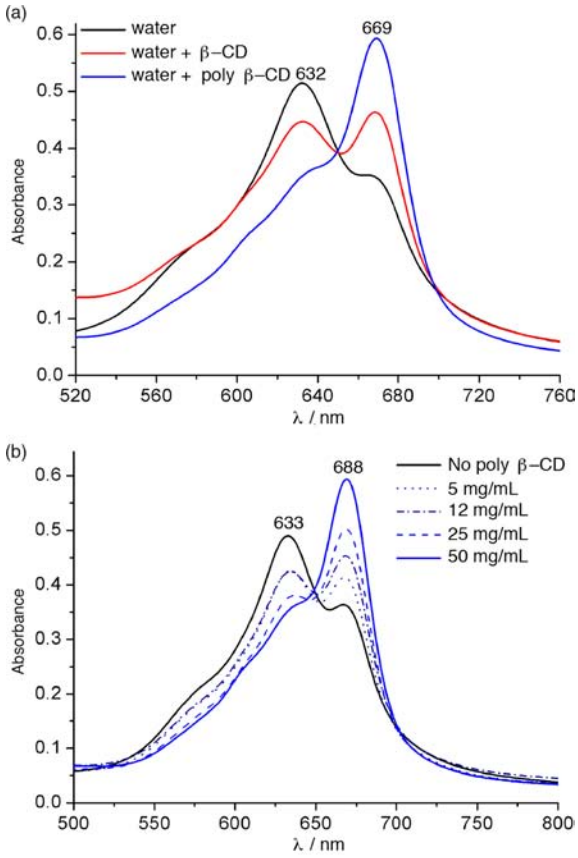

Figure 4. Absorption spectrum of **2b** in aqueous solutions containing (a) *β*-CD and poly *β*-CD; (b) different concentrations of poly-*β*CD.

values. In alkaline solution, however, the equilibrium was displaced toward monomer formation, since the dimer band decreased with increasing pH. However, from pH above 12, the monomer Q-band shifts to the red to 669 nm while the Soret band begins to lose its intensity. This change may be characteristic of Co(II)Pc, and similar results were previously reported for the water-soluble cobalt(II) tetrasulfophthalocyanine.[24]

The absorption spectra of compound **2b** was not significantly affected from pH 3.8 to 12.7. However, in very acidic media, the Soret and Q bands of both aggregated and nonaggregated species shifted to the red and decreased in intensity, with concomitant isosbestic points appearing at around 550 and 700 nm. This change suggests Fe(III)Pcs, which usually show a red-shifted Q band compared to the Fe(II) species, falling between 670 and 690 nm.[1a] However, this species is very unstable in

dx.doi.org/10.1021/ic4002048 | *Inorg. Chem.* 2013, 52, 9206−9215

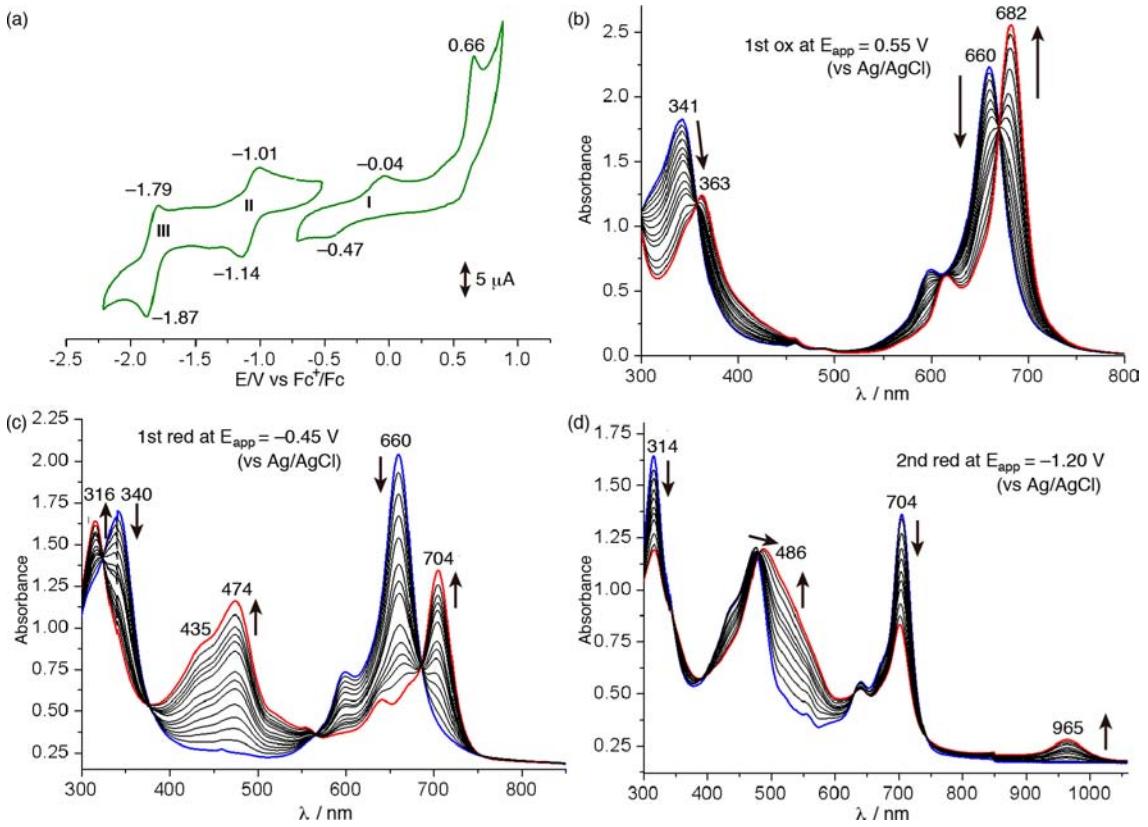

Figure 5. (a) Cyclic voltammogram of **1a** in pyridine containing TBAP (0.1 M), at a scan rate of 100 mV/s. Spectral changes of **1a** in pyridine by applying (b) 0.55, (c) −0.45, and (d) −1.2 V potentials versus Ag/AgCl reference electrode. Supporting electrolyte: TBAP 0.3 M.

solution, and further spectroscopic analysis could not be carried out (Figure S4).

Cyclic Voltammetry and Spectroelectrochemistry. Electrochemical measurements were performed to give further insight into the electronic properties of the phthalocyanines. The cyclic voltammogram (CV) of compound **1a** in pyridine is shown in Figure 5a. Two oxidation and two reduction processes can be observed. Process I shows a $\Delta(E_{pa} - E_{pc})$ higher than 60 mV and is quasireversible, suggesting a possible ligand exchange, where pyridine coordinates the metal or not. Process III is reversible, and the second oxidation process is completely irreversible. Linear curves were obtained from the plots of the square root of scan rate versus current for couples I to III, indicating diffusion controlled processes. For assignment of the redox processes, spectroeletrochemical measurements were performed and the results summarized in Figure 5b−d. When enough potential was applied for process I to occur, the Q band of **1a** red-shifted to 682 nm, followed by a red-shift and decrease in intensity of the Soret band. The clear isosbestic points formed at 356 and 668 nm indicate an equilibrium between two species in solution. Shifts of the Q band position are a typical feature of metal-centered redox processes, and since the spectral changes support the formation of Co(III)Pc species in solution,[1a,25] process I was assigned to the $Co^{II}Pc/Co^{III}Pc$ couple. At the first reduction peak of **1a**, shifts in the Soret and Q bands were also observed, and this time, two strong, broad absorptions appeared between the Soret and Q bands. Together with the weak, red-shifted Q band, these absorptions are characteristic of Co(I)Pc species in solution,[26] indicating that the couple Co(I)Pc/Co(II)Pc is responsible for process II. Upon application of more negative potentials, further reduction of the central metal or reduction of the Pc ring can occur. At process III, the spectral evolution shows a sharp depletion of the Soret and Q bands, and appearance of a new, weak band at 965 nm. As the main Pc absorptions originate from $\pi-\pi^*$ transitions in the Pc ligands, they are significantly affected by oxidation or reduction of the macrocycle. In addition, low-intensity bands in the 1000 nm region are characteristic of phthalocyanine anion radicals,[27] and hence the last process was assigned to $Co(I)Pc^{3-}/Co(I)Pc^{2-}$. The original spectra were regenerated in all cases by applying 0 V potential at the end of each measurement. All processes are electronically reversible (Figure S5).

CV and DPV of the quaternized cobalt complex **2a** in DMF are shown in Figure 6. The presence of an extra peak on the reduction path of couple II may be related to aggregates formed in the highly concentrated solution required for the experiment. Spectroelectrochemical measurements of couples I to III showed spectral changes similar to those observed for compound **1a**, and therefore, the redox processes were similarly assigned. Processes I and II are completely reversible; however, in process III, macrocyclic decomposition was eventually observed during the experiment, and the original spectrum could not be regenerated (Figure S6).

For the iron complex **1b**, one oxidation and two well-defined reduction couples can be observed in the cyclic voltammogram (Figure 7). The oxidation process is irreversible, since only ring decomposition was observed upon potential application. The plots of square wave of the scan rate versus current for couples II and III are linear, pointing to diffusion controlled processes. The spectral changes at the first reduction potential of **1b** show a sharp depletion of both the Soret and Q bands, and the

dx.doi.org/10.1021/ic4002048 | Inorg. Chem. 2013, 52, 9206−9215

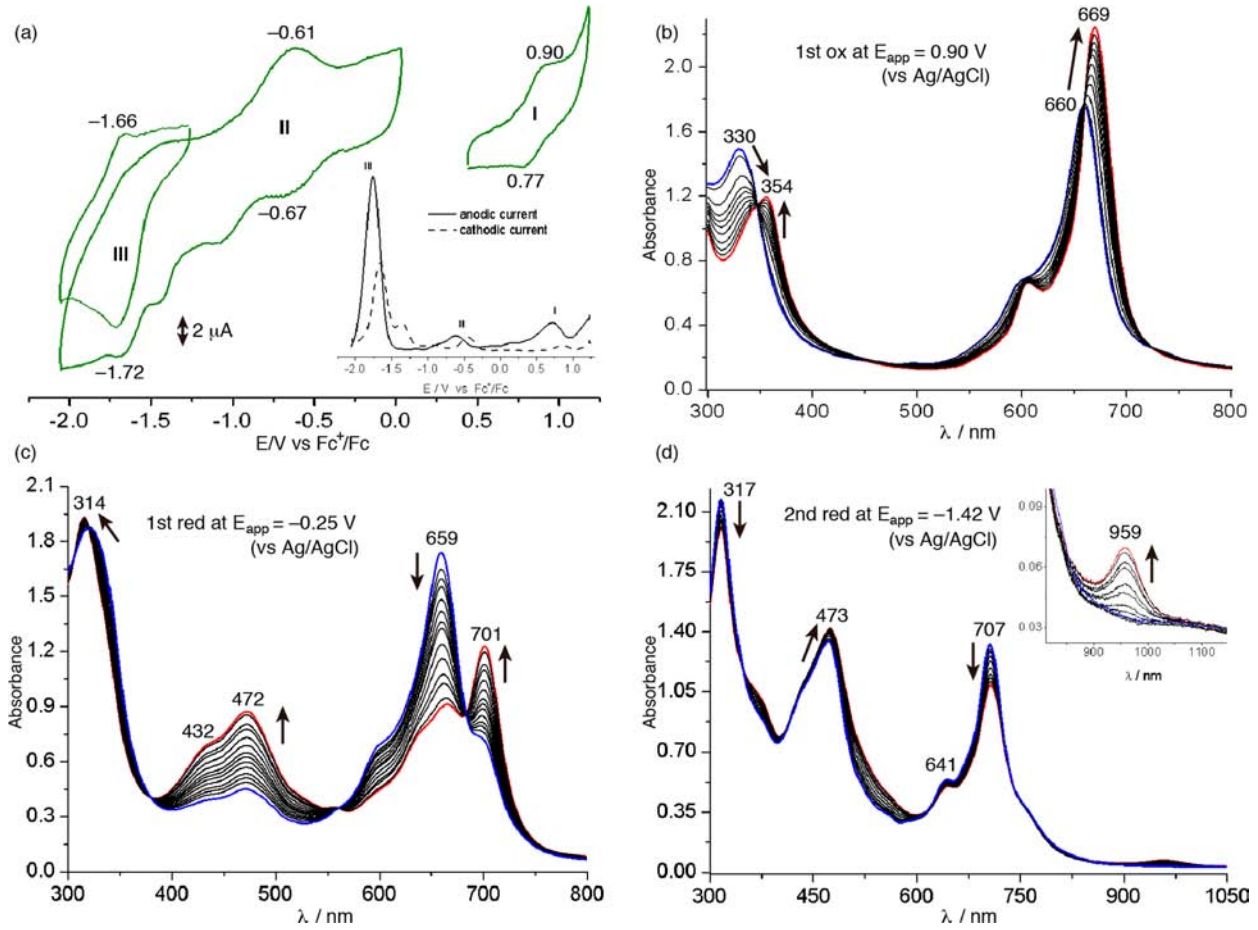

Figure 6. (a) Cyclic voltammogram and differential pulse voltammogram (inset) of **2a** in DMF containing TBAP (0.1 M), at a scan rate of 100 mV/s. Spectral changes by applying (b) 0.90, (c) −0.25, and (d) −1.42 V potentials versus Ag/AgCl reference electrode. Supporting electrolyte: TBAP 0.3 M.

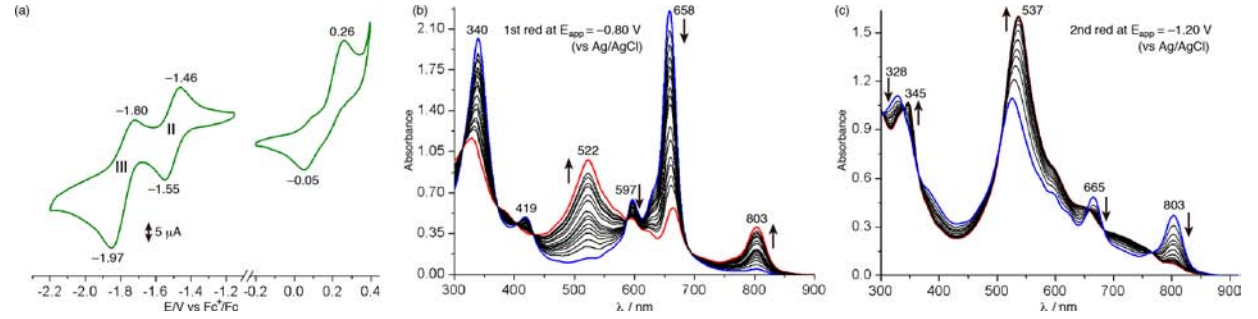

Figure 7. (a) Cyclic voltammogram of **1b** in pyridine containing TBAP (0.1 M), at a scan rate of 100 mV/s. Spectral changes of **1b** pyridine solution by applying (b) −0.80 and (c) −1.2 V potentials versus Ag/AgCl reference electrode. Supporting electrolyte: TBAP 0.3 M.

appearance of absorptions at 522 and 803 nm. Although this profile can be easily misinterpreted as a reduction centered on the Pc ring, for the same reasons explained for compound **1a**, the redox chemistry of iron phthalocyanines is not as simple and clear as the cobalt species. As previously reported, the first reduction of Fe(II)Pc occurs at ca. −1.50 V, generating a species with a sharp, moderately strong absorption in the near-infrared region, which was assigned to $Fe(I)Pc^{2-}$ with the aid of electron spin resonance (ESR) measurements.[28] In addition, the difference between the first reduction potential of compounds **1a** and **1b** is around 500 mV, while the second reductions lie at very similar potentials, which is reasonable considering they are metal and ring processes, respectively. In this sense, couples II and III were assigned to $Fe(I)Pc^{2-}$/$Fe(II)Pc^{2-}$ and $Fe(I)Pc^{3-}$/$Fe(I)Pc^{2-}$, respectively, although the possibility of mixing between metal-reduced and ring-reduced species in both processes cannot be ruled out. The original spectrum of **1b** was regenerated upon application of anodic potentials (Figure S7), confirming the reversibility of both couples.

Finally, the cyclic voltammogram of **2b** is shown in Figure 8. The broad, low-intensity peaks may be a consequence of the high aggregation level of **2a** in DMF, and may also be because of its poor solubility, which makes the diffusion of molecules toward the electrode very slow. Processes II and III, however, can be more clearly observed from the DPV plots. Process II is

dx.doi.org/10.1021/ic4002048 | Inorg. Chem. 2013, 52, 9206−9215

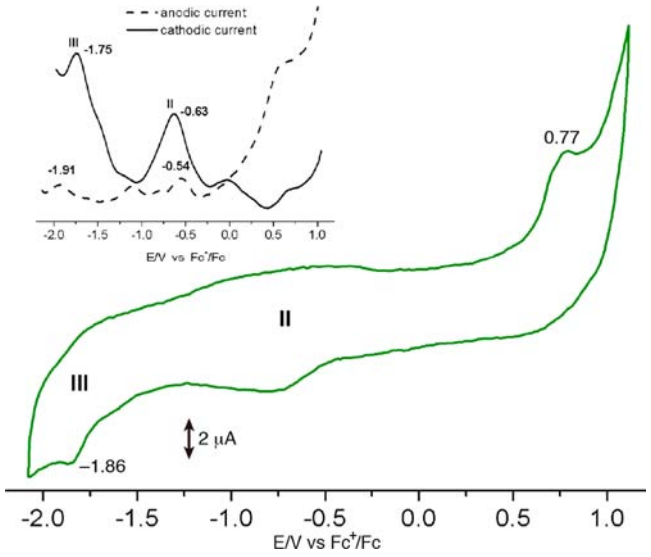

Figure 8. (A) Cyclic voltammogram and differential pulse voltammogram (inset) of **2b** in DMF containing TBAP (0.1 M), at a scan rate of 100 mV/s.

still reversible, although a lower anodic current was observed, while process III, related to reduction of the phthalocyanine ring, showed irreversibility, as also seen for the cobalt complex **2a**.

The potential values of processes I, II, and III for the four compounds are summarized in Table 1. After quaternization of the pyridyl groups, both metal processes I and II were greatly shifted to more anodic potential, with shifts reaching 1 V for the cobalt couple I and iron couple II. The redox processes of the macrocycles are little influenced by the central metal or methylation of the substituent groups. The methylation effect at the pyridyl rings is also relatively weak due to the small electronic interaction between the Pc and pyridyl rings.

Table 1. Summary of the Processes' $E_{1/2}$V Values (vs Fc^+/Fc) for All Studied Complexes

	I: M(II)Pc/ M(III)Pc	II: M(I)Pc/ M(II)Pc	III: $M(I)Pc^{3-}$/ $M(I)Pc^{2-}$
CoPyoxyPc[a]	−0.26 (0.99)	−1.06 (0.98)	−1.83 (0.99)
FePyoxyPc[a]		−1.50 (0.99)	−1.88 (0.99)
CoTMPyoxyPc[b]	0.86	−0.71	−1.70[c]
FeTMPyoxyPc[b]		−0.58	−1.86[c]

[a]Conditions: 1 mM in pyridine; TBAP (0.1M); scan rate of 100 mV s^{-1}. [b]Conditions: 1 mM in DMF; TBAP (0.1M); scan rate of 100 mV s^{-1}; Pc's counterion is perchlorate. In brackets: values of R^2 for the plot of i_p vs $\nu^{1/2}$. [c]Irreversible processes.

Electrocatalysis of the Oxygen Reduction Reaction (ORR). In order to investigate the efficiency of the studied phthalocyanines as catalysts for the oxygen reduction reaction, a monolayer film of each compound was deposited on the surface of a GC electrode and the cyclic voltammogram obtained in air-saturated aqueous solution (Figure 9). The strong, sharp cathodic peak observed in the voltammogram of each macrocycle is related to the oxygen reduction process, with the potential obtained against the Ag/AgCl electrode. A GC electrode with no Pc coating (bare electrode) shows the ORR peak at −0.53 V in acidic solution and at a more cathodic potential (−0.71 V) in alkaline solution. At low pH, the plots for the electrodes coated with **1a** and **2a** show the peak for the oxygen reduction at around −0.34 V, which is an anodic shift of about 200 mV compared to the bare electrode, hence illustrating the catalytic effect. Under the same conditions, the reaction catalysis for the films of **1b** and **2b** appears to begin at very anodic potentials (near 0 V) reaching a maximum peak current at −0.43 V. The broad shoulder observed in both voltammograms at around −0.18 V may be related to a parallel process leading to the formation of intermediate species. By increasing the scan rate for both macrocycles films (Figure S8), no significant difference in the current ratio of these two peaks was observed, which indicates that both are fast processes. In alkaline pH, however, no shoulders are observed in the plots of **1b** and **2b**, while the methylated complex shows a better catalytic effect than the unmethylated species. The opposite phenomenon is observed for the cobalt compounds **1a** and **2a**, although the potential difference between them is less pronounced.

Under a nitrogen atmosphere in acidic solution, the reduction process observed at around 0 V for both complexes is assigned to the reduction of the metal center from M(II)Pc to M(I)Pc in the films. Since this process occurs at more anodic potential than the ORR, it is reasonable to consider that the first step in the mechanism consists of an electron transfer reaction from the electrode to the Pc metal center, followed by reduction of the oxygen molecules by the complex, regenerating the catalyst.

Electroreduction of oxygen in acidic solution can occur via the following pH-dependent reaction pathways:[29]

$$O_2 + 4H^+ + 4e^- \rightarrow 2H_2O \quad (1)$$

$$O_2 + 2H^+ + 2e^- \rightarrow H_2O_2 \quad (2)$$

$$H_2O_2 + 2H^+ + 2e^- \rightarrow 2H_2O \quad (3)$$

Equation 1 represents the direct, efficient four-electron reduction of oxygen, to yield water as the final product. Incomplete reduction can also occur through a two-electron pathway, leading to a stable hydrogen peroxide species (eq 2), which can be further reduced to water at more negative potentials (eq 3). In alkaline pH, the same mechanisms are valid, although the species involved are as follows:[30]

$$O_2 + 2H_2O + 4e^- \rightarrow 4OH^- \quad (4)$$

$$O_2 + H_2O + 2e^- \rightarrow HOO^- + OH^- \quad (5)$$

$$HOO^- + H_2O + 2e^- \rightarrow 3OH^- \quad (6)$$

The ORR on the bare GC electrode proceeds through a two-electron mechanism (eq 2), and considering that, in acidic media, little difference is observed in the current intensity of the oxygen reduction peak between the bare electrode and those coated with the Pcs, we can assume that peroxide formation is being catalyzed by all compounds under these conditions. In alkaline solution, however, the coated electrodes showed increased peak current compared to the bare electrode, with a more pronounced intensity observed for the iron soluble complex **2b**, which may indicate the occurrence of a four-electron mechanism (eq 4) or an incomplete 2 + 2-electron mechanism.

In order to obtain the number of electrons involved in the ORR for the immobilized Pcs in alkaline solution, measurements using a rotating disk electrode (RDE) were performed. Figure 10 shows the voltammograms for the uncoated GC disk

dx.doi.org/10.1021/ic4002048 | Inorg. Chem. 2013, 52, 9206−9215

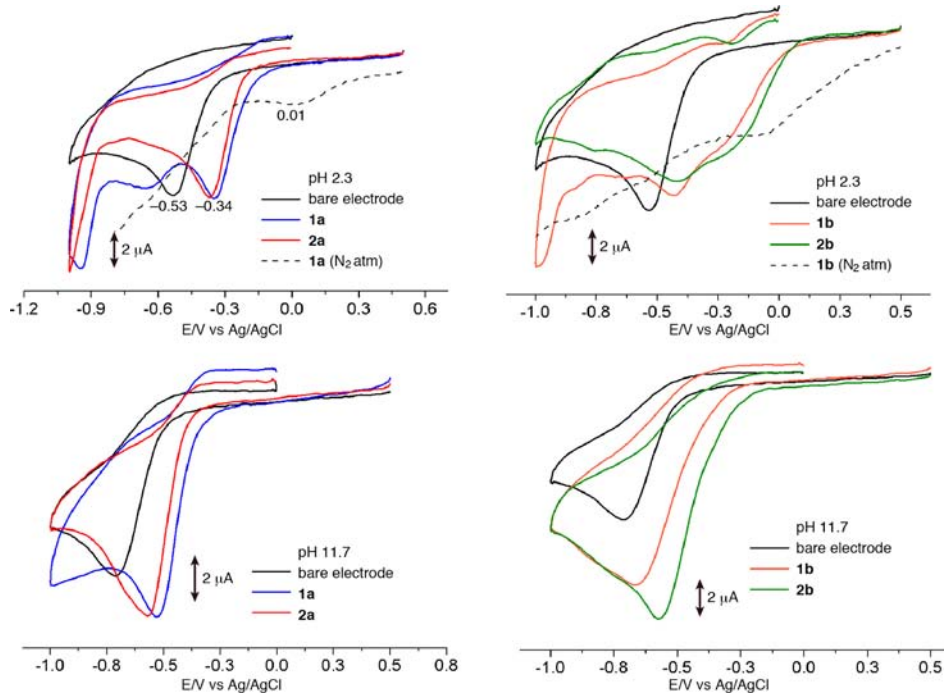

Figure 9. Cyclic voltammetry measurements of adsorbed Pcs on GC electrode for ORR catalysis. Air saturated Britton−Robinson buffers were used as electrolyte solutions. Scan rate: 100 mV/s.

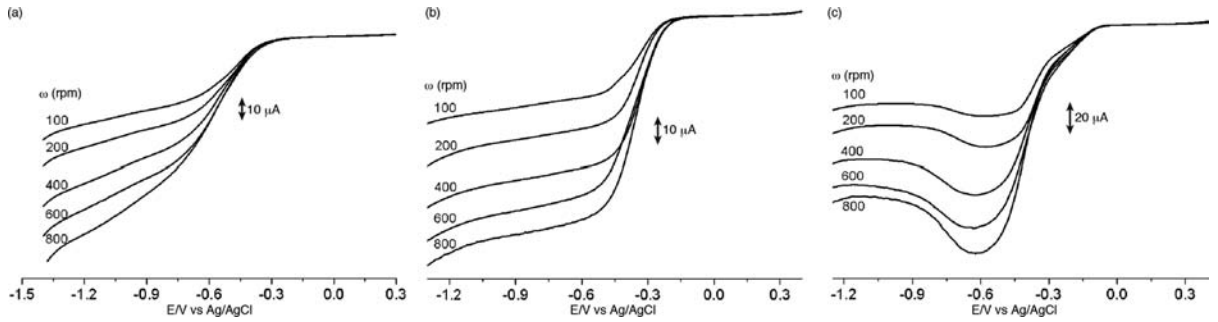

Figure 10. Rotating disk voltammetry curves for the oxygen reaction catalysis using a GC electrode in air saturated buffer solutions (pH 12). (a) Bare electrode, (b) coated with **2a**, and (c) coated with **2b**. Scan speed: 50 mV/s.

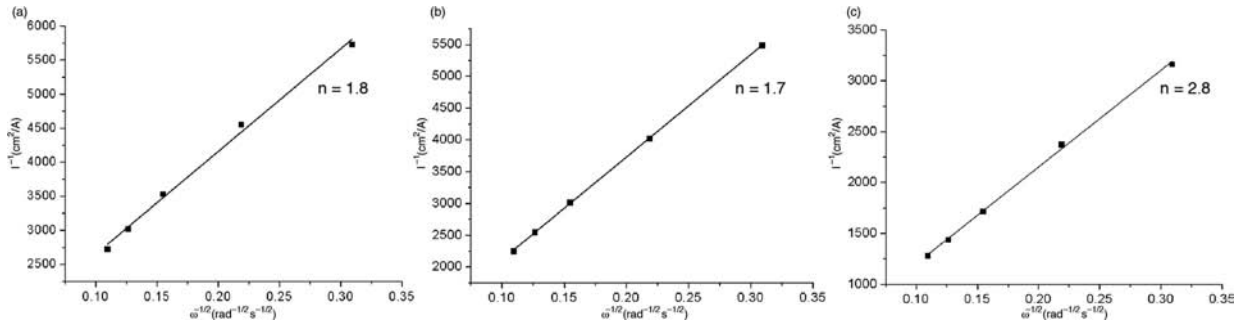

Figure 11. Levich−Koutecky plots for the ORR for the GC rotating disk electrode (a) uncoated and coated with (b) **2a** and (c) **2b**.

electrode and coated with **2a** and **2b** in air-saturated buffer solution (pH 12) at various rotation rates. In rotating disk voltammetry (RDV) experiments, the redox processes are characterized by polarization curves containing flat plateau currents from which the limiting current value i_{max} and $E_{1/2}$ (potential at which $i = 0.5i_{max}$) can be extracted.

The plot for the bare GC electrode showed a $E_{1/2}$ value of −0.52 V against −0.36 and −0.37 V obtained for **2a** and **2b**, respectively, again indicating the catalytic effect of these macrocycles. The absence of flat plateau currents at the bare electrode may be indicative of its poor catalytic activity, since all oxygen reaching the electrode cannot be accommodated in the surface, and more negative potentials are needed.[31] Macrocycles **2a** and **2b** showed more constant i_{max} values in the mass transport region, although a peak can be observed in the curves of **2b**. Considering together the CV data in Figure 9 and the

dx.doi.org/10.1021/ic4002048 | Inorg. Chem. 2013, 52, 9206−9215

CV and RDV data of tetracarboxylated FePc[32a] and other iron porphyrins,[32b,c] this may be due to the reduction of H_2O_2 occurring at or slightly more negative potentials than that of the process from O_2 to H_2O_2.

For mass transport controlled processes, the number of electrons involved in the half reactions is related to the limiting current and rotation rate, as described by the Levich equation (eq 7):

$$i_L = 0.62nFAD^{2/3}C_0\nu^{-1/6}\omega^{1/2} \quad (7)$$

Here i_L is the Levich current, n is the number of electrons transferred in the half reaction, F is the Faraday constant (96 500 C mol^{-1}), A is the electrode's area (0.196 cm^2), D is the diffusion coefficient of O_2 in the buffer solutions (1.7×10^{-5} cm^2 s^{-1}), ν is the kinematic viscosity of the solution (0.01 cm^2 s^{-1}), C_0 is the concentration of oxygen in solution (1.3×10^{-3} mol L^{-1}), and ω is the angular rotation rate of the electrode (rad s^{-1}).[10a,33]

Plots of current density (I) versus rotation rate resulted in linear curves in which the number of electrons n was calculated from the angular coefficient (Figure 11). The values of n found for the bare electrode and that coated with **2a** were 1.8 and 1.7, respectively, which indicate that the catalysis proceeds via a two-electron mechanism (eq 5), with formation of the peroxide anion. Compound **2b**, however, shows n equal to 2.8. From the data in Figures 9 and 10, this value may indicate a 2 + 2 mechanism, which consists of a first complete O_2 to H_2O_2 process and a subsequent incomplete H_2O_2 to H_2O process. This often occurs for mononuclear FePcs and iron porphyrins.[32]

In summary, we have reported the synthesis, characterization, and electronic properties of novel cobalt and iron phthalocyanines containing nonmethylated and methylated pyridyl groups. The quaternized complexes **2a** and **2b** showed enhanced water solubility, while disaggregation in aqueous solution could be achieved through different strategies. Electrochemical measurements of the compounds showed that the redox processes of the macrocycles are little influenced by the coordinated metal ion, and that, after the quaternization reaction, all of the metal redox processes are shifted greatly to more anodic potentials. All phthalocyanines immobilized on a GC electrode showed a catalytic effect for ORR. The iron compounds **1b** and **2b** showed improved catalysis in acidic media, with the reduction process starting at potentials close to 0 V. Compound **2b** also showed an increased ORR current in alkaline media, and an incomplete 2 + 2-electron reduction mechanism could be proposed from the RDE experiments. These results, allied with the simple synthetic procedure, good yields, and high stability of the compounds at both acid and alkaline pH, make them potential candidates for applications involving oxygen reduction reactions, as antibacteria and deodorant agents, and in fuel cell devices.

■ ASSOCIATED CONTENT

Supporting Information

Additional spectroscopic results of the studied phthalocyanines. This material is available free of charge via the Internet at http://pubs.acs.org.

■ AUTHOR INFORMATION

Corresponding Author

*E-mail: nagaok@m.tohoku.ac.jp.

Notes

The authors declare no competing financial interest.

■ ACKNOWLEDGMENTS

This work was partly supported by a Grant-in-Aid for Scientific Research on Innovative areas (No. 20108007, "pi-Space"), Scientific Research (B) (No. 23350095), and Young Scientist (B) (No. 24750031) from the Ministry of Education, Culture, Sports, Science, and Technology (MEXT).

■ REFERENCES

(1) (a) Leznoff, C. C.; Lever, A. B. P. *Phthalocyanines: Properties and Aplications*; VCH: New York, 1989; Vol. *1*, p 436. (b) Kadish, K. M.; Smith, K. M.; Guilard, R. *The Porphyrin Handbook*; Academic Press: San Diego, 2000. (c) Kadish, K. M.; Smith, K. M.; Guilard, R. *Handbook of Porphyrin Science*; World Scientific Publishing: Singapore, 2010.

(2) (a) Lin, C.-L.; Lee, C.-C.; Ho, K.-C. *J. Electroanal. Chem.* **2002**, *524*−*525*, 81−89. (b) Somani, P. R.; Radhakrishnan, S. *Mater. Chem. Phys.* **2002**, *77*, 117−133. (c) Green, J. M.; Faulkner, L. R. *J. Am. Chem. Soc.* **1983**, *105*, 2950−2955.

(3) (a) Oliveira, K. T. D.; Assis, F. F. D.; Ribeiro, A. O.; Neri, C. R.; Fernandes, A. U.; Baptista, M. S.; Lopes, N. P.; Serra, O. A.; Iamamoto, Y. *J. Org. Chem.* **2009**, *74*, 7962−7965. (b) Sekkat, N.; Bergh, H. V. D.; Nyokong, T.; Lange, N. *Molecules* **2012**, *17*, 98−114. (c) Jiang, X.-J.; Yeung, S.-L.; Lo, P.-C.; Fong, W.-P.; Ng, D. K. P. *J. Med. Chem.* **2011**, *54*, 320−330.

(4) (a) Laoire, C. O.; Mukerjee, S.; Abraham, K. M.; Plichta, E. J.; Hendrickson, M. A. *J. Phys. Chem. C* **2009**, *113*, 20127−20134. (b) Su, B.; Nia, R. P.; Li, F.; Hojeij, M.; Prudent, M.; Corminboeuf, C.; Samec, Z.; Girault, H. H. *Angew. Chem., Int. Ed.* **2008**, *47*, 4675−4678. (c) Wang, B. *J. Power Sources* **2005**, *152*, 1−15.

(5) (a) Morozan, A.; Jousselme, B.; Palacin, S. *Energy Environ. Sci* **2011**, *4*, 1238−1254. (b) Muller, K.; Richter, M.; Friedrich, D.; Paloumpa, I.; Kramm, U. I.; Schmeiber, D. *Solid State Ionics* **2012**, *216*, 78−82.

(6) Jasinski, R. *Nature* **1964**, *201*, 1212−1213.

(7) (a) Li, Y.; Wu, S.; Su, B. *Chem.—Eur. J.* **2012**, *18*, 7372−7376. (b) Kobayashi, M.; Niwa, H.; Harada, Y.; Horiba, K.; Oshima, M.; Ofuchi, H.; Terakura, K.; Ikeda, T.; Koshigoe, Y.; Ozaki, J.; Miyata, S.; Ueda, S.; Yamashita, Y.; Yoshikawa, H.; Kobayashi, K. *J. Power Sources* **2011**, *196*, 8346−8351. (c) Ma, J.; Liu, Y.; Zhang, P.; Wang, J. *Electrochem. Commun.* **2008**, *10*, 100−102.

(8) (a) Tanaka, A. A.; Fierro, C.; Scherson, D.; Yeager, E. B. *J. Phys. Chem.* **1987**, *91*, 3799−3807. (b) Yamada, Y.; Yoshida, S.; Honda, T.; Fukuzumi, S. *Energy Environ. Sci* **2011**, *4*, 2822−2825.

(9) Faubert, G.; Lalande, G.; Côté, R.; Guay, D.; Dodelet, J. P.; Weng, L. T.; Bertrand, P.; Dénès, G. *Electrochim. Acta* **1996**, *41*, 1689−1701.

(10) (a) Ou, Z.; Lu, A.; Meng, D.; Huang, S.; Fang, Y.; Lu, G.; Kadish, K. M. *Inorg. Chem.* **2012**, *51*, 8890−8896. (b) Huang, H.-C.; Shown, I.; Chang, S.-T.; Hsu, H.-C.; Du, H.-Y.; Kuo, M.-C.; Wong, K.-T.; Wang, S.-F.; Wang, C.-H.; Chen, L.-C.; Chen, K.-H. *Adv. Funct. Mater* **2012**, *22*, 3500−3508. (c) Dogutan, D. K.; Stoian, S. A.; McGuire, R., Jr.; Schwaibe, M.; Teets, T. S.; Nocera, D. G. *J. Am. Chem. Soc.* **2011**, *133*, 131−140.

(11) Scalise, I.; Durantini, E. N. *Bioorg. Med. Chem.* **2005**, *13*, 3037−3045.

(12) (a) Shirai, H.; Tsuiki, H.; Masuda, E.; Koyama, T.; Hanabusa, K.; Kobayashi, N. *J. Phys. Chem.* **1991**, *95*, 417−423. (b) Tsuiki, H.; Masuda, E.; Koyama, T.; Hanabusa, K.; Shirai, H.; Kobayashi, N.; Minamide, N.; Komatsu, Y.; Yokozeki, T. *Polymer* **1996**, *37*, 3637−3642. (c) Shirai, H.; Maruyama, A.; Takano, J.; Kobayashi, K.; Hojo, N.; Urushido, K. *Makromol. Chem* **1980**, *181*, 565−573. (d) Shirai, H.; Maruyama, A.; Kobayashi, K.; Hojo, N.; Urushido, K. *Makromol. Chem.* **1980**, *181*, 575−584.

(13) (a) Durmus, M.; Ahsen, V. *J. Inorg. Biochem.* **2010**, *104*, 297−309. (b) Li, H.; Jensen, T. J.; Fronczek, F. R.; Vicente, G. H. *J. Med.*

Chem. **2008**, *51*, 502−511. (c) Banfi, S.; Caruso, E.; Buccafurni, L.; Ravizza, R.; Gariboldi, M.; Monti, E. *J. Organomet. Chem.* **2007**, *692*, 1269−1276. (d) Chidawanyika, W.; Ogunsipe, A.; Nyokong, T. *New J. Chem.* **2007**, *31*, 377−384. (e) Michelsen, U.; Kliesch, H.; Schnurpfeil, G.; Sobbi, A. K.; Wöhrle, D. *Photochem. Photobiol.* **1996**, *64*, 694−701. (f) Wöhrle, D.; Schnurpfeil, G.; Knothe, G. *Dyes Pigm.* **1992**, *18*, 91−102.

(14) Britton, H. T. K.; Robinson, R. A. *J. Chem. Soc.* **1931**, 1456−1462.

(15) Gaspard, S.; Tran-Thi, T. H. *J. Chem. Soc., Perkin Trans. 2* **1989**, 383−389.

(16) Metz, J.; Schneider, O.; Hanack, M. *Inorg. Chem.* **1984**, *23*, 1065−1071.

(17) Masilela, N.; Nyokong, T. *Dyes Pigm.* **2010**, *84*, 242−248.

(18) Mckeown, N. B. *Phthalocyanine Materials: Synthesis, Structure and Function*; Cambridge University Press: Cambridge, U.K., 1998; p 193.

(19) Snow, A. W. In *Porphyrin Handbook*, Kadish, K. M., Smith, K. M., Guilard, R., Eds.; Academic Press: San Diego, 2000; Vol. *17*, pp 129−173.

(20) Kasha, M.; Rawls, H. R.; El-Bayoumi, M. A. *Pure Appl. Chem.* **1965**, *11*, 371−392.

(21) (a) Dodsworth, E. S.; Lever, A. B. P.; Seymour, P.; Leznoff, C. C. *J. Phys. Chem.* **1985**, *89*, 5698−5705. (b) Gouterman, M.; Holten, D.; Lieberman, E. *Chem. Phys.* **1977**, *25*, 139−153.

(22) Reichardt, C. *Solvents and Solvent Effects in Organic Chemistry*, 4th ed.; Wiley-VCH: Weinhein, Germany, 2011.

(23) (a) Mosinger, J.; Deumié, M.; Lang, K.; Kubát, P.; Wagnerová, D. M. *J. Photochem. Photobiol., A* **2000**, *130*, 13−20. (b) Tau, P.; Ogunsipe, A. O.; Maree, S.; Maree, M. D.; Nyokong, T. *J. Porphyrins Phthalocyanines* **2003**, *7*, 439−446.

(24) Lever, A. B. P.; Hempstead, M. R.; Leznoff, C. C.; Liu, W.; Melnik, M.; Nevin, W. A.; Seymour, P. *Pure Appl. Chem.* **1986**, *58*, 1467−1476.

(25) Gunsel, A.; Kandaz, M.; Koca, A.; Salih, B. *Polyhedron* **2011**, *30*, 1446−1455.

(26) Kobayashi, N.; Miwa, H.; Nemykin, V. N. *J. Am. Chem. Soc.* **2002**, *124*, 8007−8020.

(27) (a) Ou, Z.; Zhan, R.; Tomachynski, L. A.; Chernii, V. Y.; Kadish, K. M. *Macroheterocycles* **2011**, *4*, 164−170. (b) Mack, J.; Stillman, M. J. *J. Am. Chem. Soc.* **1994**, *116*, 1292−1304.

(28) Lever, A. B. P.; Wilshire, J. P. *Inorg. Chem.* **1978**, *17*, 1145−1151.

(29) (a) Blizanac, B. B.; Ross, P. N.; Markovic, N. M. *Electrochim. Acta* **2007**, *52*, 2264−2271. (b) Schechter, A.; Stanevsky, M.; Mahammed, A.; Gross, Z. *Inorg. Chem.* **2012**, *51*, 22−24.

(30) Schmidt, T. J.; Stamenkovic, V.; Arenz, M.; Markovic, N. M.; Ross, P. N. *Electrochim. Acta* **2002**, *47*, 3765−3776.

(31) Jiang, R.; Anson, F. C. *J. Electroanal. Chem.* **1991**, *305*, 171−184.

(32) (a) Kobayashi, N.; Nishiyama, Y. *J. Phys. Chem.* **1985**, *89*, 11671170. (b) Kobayashi, N.; Osa, T. *J. Electroanal. Chem.* **1983**, *157*, 269−281. (c) Kobayashi, N.; Nishiyama, Y. *J. Electroanal. Chem.* **1984**, *181*, 107−117. (d) Kobayashi, N.; Sudo, K.; Osa, T. *Bull. Chem. Soc. Jpn.* **1990**, *63*, 571−575.

(33) (a) Chen, R.; Li, H.; Chu, D.; Wang, G. *J. Phys. Chem. C* **2009**, *113*, 20689−20697. (b) Zhang, J.; Anson, F. C. *J. Electroanal. Chem.* **1992**, *341*, 323−341. (c) Bard, A.; Faulkner, L. R. *Electrochemical Methods: Fundamentals and Applications*, 2nd ed.; John Wiley & Sons: New York, 2001; p 856.